High-quality-factor double Fabry–Perot plasmonic nanoresonator

Baptiste Fix, Julien Jaeck, Patrick Bouchon, Sébastien Héron, Benjamin Vest, Riad Haïdar

Optics Letters

High-quality-factor double Fabry–Perot plasmonic nanoresonator

Baptiste Fix,[1] Julien Jaeck,[1,*] Patrick Bouchon,[1] Sébastien Héron,[1] Benjamin Vest,[1] and Riad Haïdar[1,2]

[1]ONERA—The French Aerospace Lab, Chemin de la Hunière, 91761 Palaiseau Cedex, France
[2]École Polytechnique, Département de Physique, 91128 Palaiseau, France
*Corresponding author: julien.jaeck@onera.fr

Received 29 September 2017; accepted 17 October 2017; posted 27 October 2017 (Doc. ID 308258); published 5 December 2017

Fabry–Perot (FP)-like resonances have been widely described in nanoantennas. In the original FP resonator, a third mirror can be added, resulting in a multimirror interferometer. However, in the case of a combination of nanoantennas, it has been reported that each cavity behaves independently. Here, we evidence the interferences between two FP absorbing nanoantennas through a common mirror, which has a strong impact on the optical behavior. While the resonance wavelength is only slightly shifted, the level of absorption reaches nearly 100%. Moreover, the quality factor increases up to factor 7 and can be chosen by geometric design over a range from 11 to 75. We demonstrate, thanks to a simple analytical model, that this coupling can be ascribed to a double FP cavity resonance, with the unique feature that each cavity is separately coupled to the outer medium.

OCIS codes: (050.6624) Subwavelength structures; (130.3060) Infrared; (310.6628) Subwavelength structures, nanostructures; (160.3918) Metamaterials.

https://doi.org/10.1364/OL.42.005062

The Fabry–Perot (FP) interferometer was invented in 1899 and consisted of two parallel highly reflecting mirrors, the resonance behavior being characterized by peaks or dips in the transmission and reflection spectra [1]. It has been used in a variety of devices, among which are optical cavities for lasers or filters [2]. Since this seminal work, various evolutions of the FP interferometer have been introduced, among which are multimirror FPs that give birth to a coherent superposition of all the beams [3]. Noteworthy, in most configurations, the mirrors are placed in series. In the past two decades, the development of nanophotonics has given birth to FP-like resonators [4–7], in which a guided mode in a metallic cavity has a behavior that is well described by the FP formalism. The advantages of these nanoresonators are their compactness and the possibility to combine them to design broadband or multiband resonances. It is well accepted that, since these metallic cavities are the siege of localized resonances, they have negligible influences on each other when they are combined [8–12]. The two most common plasmonic nanostructures with a FP behavior are the metal–insulator–metal patch nanoantennas (horizontal resonance) and the high-aspect-ratio nanogrooves (vertical resonance). Both of these resonators are promising for applications ranging from thermal emission [12,13] or infrared detection [14] to biosensing [15,16]. Yet, they suffer from their low quality factor.

In this Letter, we introduce a double-cavity FP-like nanoresonator. It departs from the previous work on multimirror FP resonators, as the mirrors are in a hybrid configuration between series and parallel. It gives birth to a spectacular effect where critical coupling (a zero of reflectivity) is obtained while, independently, each of the two cavities is loosely coupled to free space. Moreover, the quality factor of the double-cavity resonators is increased from 11 to 50, well beyond the limit for FP plasmonic nanoresonators [10]. We developed an analytical model that confirms the multimirror FP behavior. Last, but not least, while previous works reported critical coupling only in high-aspect-ratio nanogrooves (i.e., h/w is typically higher than 10), here, the critically coupled nanoresonator aspect ratio is on the order of 2.

The classical nanocavity antenna with vertical FP resonance consists of a high-aspect-ratio groove (width w, height h) etched in gold, with a subwavelength period d, as depicted in Fig. 1(a). The gold is modeled using a Drude formula [17]: $\varepsilon(\lambda) = 1 - [(\lambda_p/\lambda + i\gamma)\lambda_p/\lambda]^{-1}$ with $\lambda_p = 158.9$ nm and $\gamma = 0.0077$. The resonance wavelength of the nanogroove antenna is given by $\lambda_r \simeq 2hn_{\text{eff}}$, where n_{eff} is the effective index of the propagative mode in the groove. Thus, it is mainly dictated by the height of the groove, even if the width impacts the effective index for small values [18]. The coupling of these cavities to free space depends on the aperture ratio (w/d): the critical coupling (a zero of reflectivity) is achieved for a small aperture ratio while a larger one results in a loose coupling.

The electromagnetic analysis of these nanostructures is performed in the following of the Letter with the B-spline modal method, which allows fast and exact computations on a nonuniform mesh [19]. The reflectivity spectra of two arrays, with the same period $d = 1$ μm but different geometries for the grooves, are plotted in Fig. 1(b). For the wider groove case

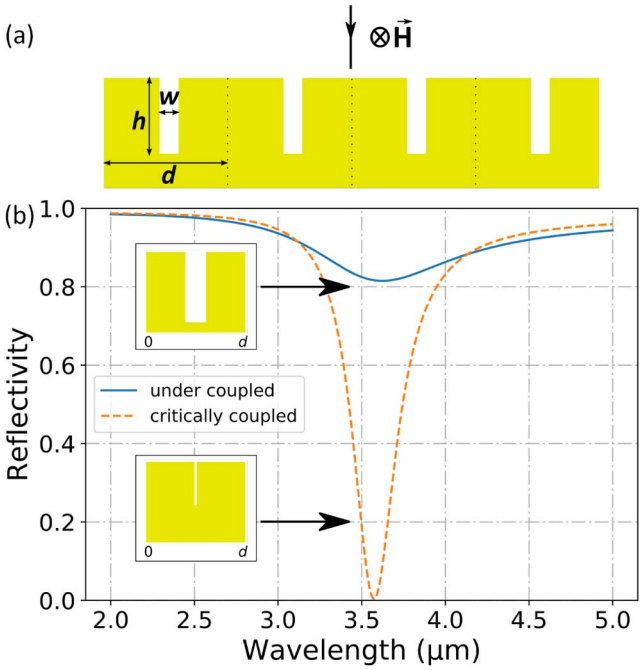

Fig. 1. (a) Scheme of the nanogrooves (width w, height h) grating (period d) illuminated with normally incident, TM-polarized light. (b) Reflectivity spectra of a loosely coupled nanogroove (blue continuous line) with width $w = 200$ nm and height 700 nm, and of a critically coupled nanogroove (orange dashed line) with width $w = 21$ nm and height 440 nm. Both gratings have the same periodicity $P = 1$ μm, and have the same resonance wavelength $\lambda_r = 3.6$ μm. The loosely coupled nanogroove absorption is smaller than 20%, while it reaches 100% for the critical coupling situation.

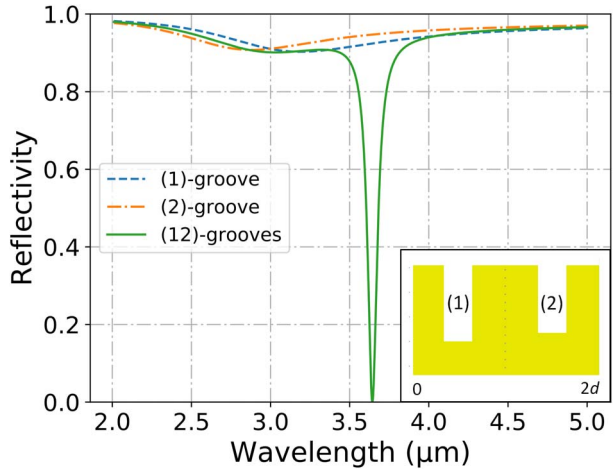

Fig. 2. Comparison between the reflectivity of two loosely coupled nanogroove resonators and the reflectivity of a critically coupled resonator composed of the two aforementioned cavities. The two individual cavities [respectively named (1) and (2)] are defined by $d = 1$ μm, $w = 300$ nm and respective heights of $h^{(1)} = 620$ nm and $h^{(2)} = 550$ nm. The reflectivities of these two nanogroove resonators are represented on dashed lines and do not go below 85%. When we change the height of one in every two slits from $h^{(1)}$ to $h^{(2)}$ as depicted in the inset, we see an unexpected modification of the periodic structure reflectivity. It drops to zero and has a 4 times higher quality factor than a single critically coupled nanogroove resonator.

($w = 200$ nm, $h = 700$ nm), the absorption (i.e., $1 - R$) is smaller than 20% at the resonance wavelength $\lambda_r = 3.6$ μm. In order to reach 100% of absorption (i.e., the critical coupling case), the width of the groove has to be reduced to $w = 21$ nm. This increases the effective index n_{eff}, so for the sake of comparison, the height of the groove is decreased to $h = 440$ nm in order to exhibit the same resonance wavelength.

It must be emphasized that the aspect ratio of the critically coupled nanoantenna is nearly 21, and its experimental realization, even if previously achieved [7,13,20], remains challenging and hinders its use in practical applications. Besides, since these cavities are the siege of localized resonances, it has been previously reported that they behave independently when they are combined [8–12]. Yet, these considerations focused only on critically coupled cavities, leaving the combination of loosely coupled nanogroove resonators unstudied.

A two-grooves system is investigated, where each individual groove is loosely coupled and is designated in the following by (1) or (2), while the combination is designated by (12). The (1)-groove [resp. (2)-groove] array has a width $w = 300$ nm, a height $h^{(1)} = 620$ nm (resp. $h^{(2)} = 550$ nm), and a period $d = 1$ μm and exhibits a loosely coupled resonance at $\lambda = 2.7$ μm (resp. $\lambda = 3.2$ μm), with a reflectivity dip at 90%, as shown in Fig. 2. The (12)-groove combines these two grooves with a period $d^{(12)} = 2d = 2$ μm, while the grooves are equidistant. The choice of this period allows keeping the same aperture ratio, and thus the same entrance mirror as the one of the individual cavities. The reflectivity spectrum of the (12)-groove is also plotted in Fig. 2 (blue continuous line), and its behavior strongly deviates from the individual grooves or their combination. Indeed, the (12)-groove structure is in critical coupling at a wavelength of $\lambda = 3.6$ μm, which represents a noticeable red shift as compared to the resonances of the (1)-groove or (2)-groove arrays. Besides, the resonance quality factor shows a fourfold increase. In this particular example, $Q = 50$ when the value for the critically coupled single FP resonator shown in Fig. 1 is $Q = 11$. This critical coupling is scalable to other wavelength ranges.

To investigate the origin of this new resonance, an analytical model is introduced, as represented in Fig. 3. There is only one propagating mode in each groove [21], and its coupling to the incoming plane wave is given by the scalar Fresnel coefficients at the interface A–B: t_{AB}, t_{BA}, r_{BB}. Inside the first (resp. second) groove, the mode propagator element is $P^{(1)}$ (resp. $P^{(2)}$), and the bottom reflection on the metallic surface is ρ. Eventually, the coupling between the two cavities is given by the scalar value (t_{BB}). It is noteworthy that, due to the choice of a simplified geometry (identical width w, and equidistant grooves), all these coefficients (except the propagators) are identical for the two grooves. Still, the analytical model can be generalized to the combination of two different grooves.

At equilibrium, straightforward algebra leads to the device reflectivity as a function of these scalar elements:

$$R = |r_{\text{AA}} + G_1 t_{\text{AB}} t_{\text{BA}} + G_2 t_{\text{AB}} t_{\text{BA}}|^2, \tag{1}$$

$$\begin{cases} G_1 = (G_1 r_{\text{BB}} + t_{\text{BA}} + G_2 t_{\text{BB}}) P_1^2 \rho \\ G_2 = (G_2 r_{\text{BB}} + t_{\text{BA}} + G_1 t_{\text{BB}}) P_2^2 \rho \end{cases}. \tag{2}$$

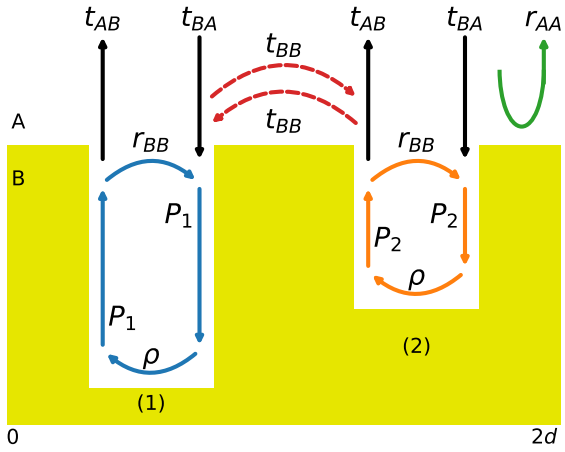

Fig. 3. Scheme of the two-groove structure and of the different coefficients used in the analytical model. All of the reflectivity (r_{AA}, r_{BB}, and ρ) and transmission coefficients (t_{AB}, t_{BA}, and t_{BB}) are scalar elements from S-matrices, and P_1 (resp. P_2) is the mode propagator element inside the first (resp. second) groove.

By resolving the previous two coupled equations, G_1 and G_2 can be expressed as

$$\begin{cases} G_1 = \frac{\rho P_1^2[1+\rho P_2^2(t_{BB}-r_{BB})]}{(1-\rho r_{BB}P_1^2)(1-\rho r_{BB}P_2^2)-t_{BB}^2\rho^2P_1^2P_2^2} \\ G_2 = \frac{\rho P_2^2[1+\rho P_1^2(t_{BB}-r_{BB})]}{(1-\rho r_{BB}P_1^2)(1-\rho r_{BB}P_2^2)-t_{BB}^2\rho^2P_1^2P_2^2} \end{cases}. \quad (3)$$

In Eq. (1), the reflection amplitude writes as the sum of three terms: the scalar reflection r_{AA} on the patterned metallic mirror and the two waves coming out from each aperture ($G_1 t_{AB}t_{BA}$ and $G_2 t_{AB}t_{BA}$), where G_1 and G_2 describe the back and forth reflections in each groove, as well as the coupling between the two grooves. It must be emphasized that in the usual case where there is no coupling, $t_{BB} = 0$, then G_i is reduced to $\frac{\rho P_i^2}{1-\rho r_{BB}P_i^2}$, giving the usual FP expression.

The comparison between the reflectivity spectra obtained with the model and with full numeric resolution of the Maxwell equations for the previous structure is plotted in Fig. 4(a). It shows an excellent agreement, which confirms both the validity of the one-mode model and that the optical behavior is due to the coupling t_{BB} between the two resonators. This simplified model also proves useful to optimize the respective height of each groove. Indeed, the scalar Fresnel coefficients and the effective index of the propagative mode have to be numerically computed, but they do not depend on the heights of the grooves. Only the propagators depend on the height, but with the following exact analytical expression: $P_{(i)} = \exp(\mathrm{i}n_{\mathrm{eff}}^{(i)}h^{(i)})$.

This critically coupled resonance can be explained by a three-plane-wave interference between the wave directly reflected on the metallic interface and the two plane waves that are exiting the two metallic cavities, after having encountered multiple backward and forward reflections in the two cavities. The phase difference and the amplitude of each of them are plotted in Figs. 4(b) and 4(c) as a function of the wavelength. As can be seen, r_{AA} is nearly spectrally independent, and so the interference can be reduced to the contributions $G_1 t_{AB}t_{BA}$ and $G_2 t_{AB}t_{BA} + r_{AA}$. Critical coupling can be achieved under two

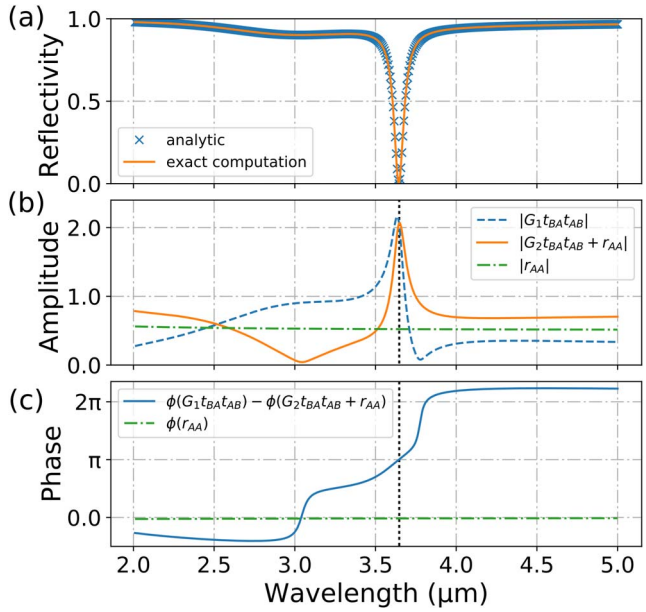

Fig. 4. (a) Comparison between the reflectivity spectrum computed by the B-spline modal method (continuous line) and the reflectivity spectrum computed from the analytical expression in Eq. (1) (dashed line with crosses). (b) Amplitude and (c) phase difference of the three terms involved in the reflectivity expression [see Eq. (1)] as a function of the wavelength. The reflectivity of the patterned metallic mirror r_{AA} remains constant in modulus and phase from 2 μm to 5 μm. At the resonance, the two conditions for a destructive interference are met: the phase difference is equal to π, and the amplitudes are equal. G_1 and G_2 are maximal near the resonance due to a minimum of their common denominator.

conditions: (i) $|G_1 t_{AB}t_{BA}|$ and $|G_2 t_{AB}t_{BA} + r_{AA}|$ must be equal, and (ii) they must be in opposite phase. As shown in Fig. 4(b), the two terms have the same amplitude at 3.6 μm and 2.5 μm, yet [see Fig. 4(c)] they are in opposite phase at 3.6 μm only. The two terms G_1 and G_2 are maximal near the resonance due to a minimum of their common denominator and the proximity of its complex pole.

As can be deduced from Eq. (1), the two grooves must have different heights for the resonance to be possible. Indeed, if the two grooves are identical, Eq. (1) reduces to $R = |r_{AA} + 2G_1 t_{AB}t_{BA}|^2$, and the only solution to achieve the critical coupling is for the single groove to be critically coupled by itself.

Eventually, the influence of the groove width is investigated. Reflectivity diagrams in the 2–5 μm range are plotted as a function of the grooves' width w for both the one-groove (height $h^{(1)}$) in Fig. 5(a) and the two-groove structure in Fig. 5(b). Dashed lines are highlighting the near-critical coupling zone for the single-groove system ($w < 100$ nm), and the specific case investigated in the Letter ($w = 300$ nm).

For thin grooves ($w < 100$ nm), the single groove is near the critical coupling condition, and exhibits a resonance wavelength that is blue shifted when w is increased. This dependence is due only to the expression of the effective index $n_{\mathrm{eff}} \simeq 1 + \frac{\delta}{w}$, where δ is the skin depth of the metal [18,22]. The two-groove structure exhibits two resonances in this zone; both are also near critical coupling and can be described as

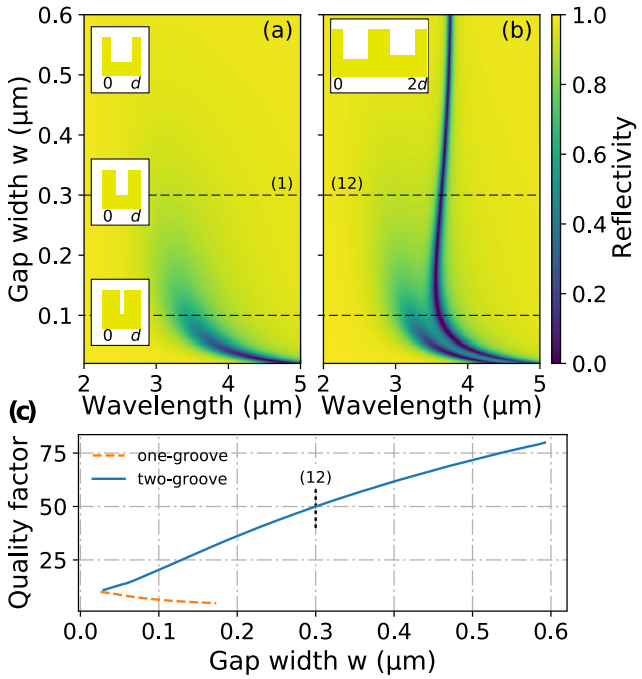

Fig. 5. Reflectivity diagram of the (a) one-groove structure (height $h^{(1)}$) and (b) two-groove structure as a function of the groove width w in the 2–5 μm spectral range. Dashed lines are highlighting the near-critical coupling zone for the one-groove system ($w < 100$ nm), and the specific case investigated previously in the Letter ($w = 300$ nm). (c) Evolution of the quality factor of the one-groove (dashed curve) and two-groove (plain curve) resonance as a function of the grooves' widths. The quality factor of the two-groove resonance keeps rising.

behaving independently. This can also be explained using the model: since each groove is independently near critical coupling, it means that the two mirrors of the cavities are good reflectors ($r_{BB} \simeq 1$). So there is nearly no transmission to the other groove ($t_{BB} \simeq 0$) and subsequently no coupling. For wider slits ($w > 100$ nm), the single groove is loosely coupled, and its reflectivity at resonance increases above 60%, and for $w > 300$ nm, the resonance is no longer distinguishable on the diagram. In the two-groove structure, one of the resonances fades away as the width is increased in the same manner as the single-groove resonator, while the other resonance remains in critical coupling. In this case, the reflectivity r_{BB} is decreasing, while t_{BB} is continuously increasing, and in Eq. (3), $t_{BB} - r_{BB}$ cannot be simplified anymore. Thus, as the width increases, both grooves are more and more coupled to each other. Noteworthy, the resonance wavelength is nearly independent of w ($\lambda_r = 3.5$ μm for $w = 100$ nm and $\lambda_r = 3.7$ μm for $w = 600$ nm). This is particularly appealing from the technological point of view, since the aspect ratio of the grooves can be decreased to one, making their fabrication much less of a challenge. Moreover, as shown in Fig. 5(c), the quality factor continuously rises with the gap width, so that it can be chosen, independently from the wavelength, by geometric design over a range from 11 to 75. In this particular case, it is the resonance associated with the smaller groove that seems to fade away, but this is in fact completely determined by the coupling between the two grooves t_{BB}. This last term can be engineered, for instance, by modifying the distance between the two grooves (while maintaining the same period), so that the second resonance fades away while the first is critically coupled.

To conclude, the coupling between two loosely coupled FP-like resonators leads to a promising behavior, where the quality factor is strongly increased, and critical coupling is obtained for low-aspect-ratio grooves. An analytical description of the two-grooves system has ascribed the resonance behavior to interferences due to an equivalent three-mirrors FP system, and a similar approach can be used for a higher number of mirrors or for other kinds of FP nanoantennas. This approach can be generalized to multicavities, which can be used to expand this effect on multi-band resonances, and it can also be applied to transmission devices. This description also paves the way to the manipulation and the engineering of the equivalent mirror coupling of the two nanocavities, in order to reach multimirror interferences theory predictions. This structure is also very promising for practical applications of the nanogroove system, as it relaxes the technological constraints on the groove (wider aperture, lower aspect ratio).

Funding. DGA-MRIS scholarship.

REFERENCES

1. C. Fabry and A. Perot, Ann. Chim. Phys **16**, 115 (1899).
2. E. Schubert, N. Hunt, M. Micovic, R. Malik, D. Sivco, A. Cho, and G. Zydzik, Science **265**, 943 (1994).
3. H. Van de Stadt and J. M. Muller, J. Opt. Soc. Am. A **2**, 1363 (1985).
4. J. Porto, F. Garcia-Vidal, and J. Pendry, Phys. Rev. Lett. **83**, 2845 (1999).
5. J. Dorfmüller, R. Vogelgesang, R. T. Weitz, C. Rockstuhl, C. Etrich, T. Pertsch, F. Lederer, and K. Kern, Nano Lett. **9**, 2372 (2009).
6. E. Cubukcu and F. Capasso, Appl. Phys. Lett. **95**, 201101 (2009).
7. P. Bouchon, F. Pardo, B. Portier, L. Ferlazzo, P. Ghenuche, G. Dagher, C. Dupuis, N. Bardou, R. Haïdar, and J. Pelouard, Appl. Phys. Lett. **98**, 191109 (2011).
8. X. Liu, T. Starr, A. Starr, and W. Padilla, Phys. Rev. Lett. **104**, 207403 (2010).
9. P. Bouchon, C. Koechlin, F. Pardo, R. Haïdar, and J.-L. Pelouard, Opt. Lett. **37**, 1038 (2012).
10. C. Koechlin, P. Bouchon, F. Pardo, J.-L. Pelouard, and R. Hadar, Opt. Express **21**, 7025 (2013).
11. Y. Cui, Y. He, Y. Jin, F. Ding, L. Yang, Y. Ye, S. Zhong, Y. Lin, and S. He, Laser Photon. Rev. **8**, 495 (2014).
12. M. Makhsiyan, P. Bouchon, J. Jaeck, J.-L. Pelouard, and R. Hadar, Appl. Phys. Lett. **107**, 251103 (2015).
13. H. Miyazaki, K. Ikeda, T. Kasaya, K. Yamamoto, Y. Inoue, K. Fujimura, T. Kanakugi, M. Okada, K. Hatade, and S. Kitagawa, Appl. Phys. Lett. **92**, 141114 (2008).
14. M. Knight, H. Sobhani, P. Nordlander, and N. Halas, Science **332**, 702 (2011).
15. A. Cattoni, P. Ghenuche, A. Haghiri-Gosnet, D. Decanini, J. Chen, J. Pelouard, and S. Collin, Nano Lett. **11**, 3557 (2011).
16. A. Dhawan, M. Canva, and T. Vo-Dinh, Opt. Express **19**, 787 (2011).
17. E. Palik and G. Ghosh, *Handbook of Optical Constants of Solids* (Academic Press, 1985).
18. S. Collin, F. Pardo, and J.-L. Pelouard, Opt. Express **15**, 4310 (2007).
19. P. Bouchon, F. Pardo, R. Haïdar, and J. Pelouard, J. Opt. Soc. Am. A **27**, 696 (2010).
20. Y.-K. R. Wu, A. E. Hollowell, C. Zhang, and L. J. Guo, Sci. Rep. **3**, 1194 (2013).
21. P. Lalanne, J. Hugonin, S. Astilean, M. Palamaru, and K. Möller, J. Opt. A **2**, 48 (2000).
22. S. Héron, P. Bouchon, and R. Hadar, Phys. Rev. A **94**, 033831 (2016).